SEDIMENTOLOGY
the journal of the
International Association of Sedimentologists

Mineralogy and geochemistry of atypical reduction spheroids from the Tumblagooda Sandstone, Western Australia

Journal:	*Sedimentology*
Manuscript ID	SED-2019-OM-038.R1
Manuscript Type:	Original Manuscript
Date Submitted by the Author:	08-Jul-2019
Complete List of Authors:	Fox, David; Commonwealth Scientific and Industrial Research Organisation, Mineral Resources; Curtin University, School of Earth and Planetary Sciences Spinks, Sam; Commonwealth Scientific and Industrial Research Organisation, Mineral Resources Thorne, Robert; Commonwealth Scientific and Industrial Research Organisation, Mineral Resources Barham, Milo; Curtin University, Department of Applied Geology Aspandiar, Mehrooz; Curtin University, School of Earth and Planetary Sciences Armstrong, Joseph; University of Aberdeen, Geology and Petroleum Geology; Commonwealth Scientific and Industrial Research Organisation, Mineral Resources Uysal, Tonguc; Commonwealth Scientific and Industrial Research Organisation, Energy Timms, Nick; Curtin University, Department of Applied Geology Pearce, Mark; Commonwealth Scientific and Industrial Research Organisation, Mineral Resources Verrall, Michael; Commonwealth Scientific and Industrial Research Organisation, Mineral Resources Godel, Belinda; Commonwealth Scientific and Industrial Research Organisation, Mineral Resources Whisson, Brad; LabWest Minerals Analysis Pty Ltd
Keywords:	Red beds, Diagenesis, Redox, Carnarvon Basin, Metal-reducing bacteria, Haematite, Perth Basin, Svanbergite

Note: The following files were submitted by the author for peer review, but cannot be converted to PDF. You must view these files (e.g. movies) online.

KAL17_1 XRD.svg
KAL17_29 XRD.svg
4_SHARP_0017_simple_volume_rendering.mpg
37_SHARP_0018_3D_movie1.mpg

Mineralogy and geochemistry of atypical reduction spheroids from the Tumblagooda Sandstone, Western Australia

David C. M. Fox[1,2], Samuel C. Spinks[1], Robert L. Thorne[1], Milo Barham[2,3], Mehrooz Aspandiar[2], Joseph G. T. Armstrong[1,4], Tonguç Uysal[5], Nicholas E. Timms[2], Mark A. Pearce[1], Michael Verrall[1], Belinda Godel[1], Brad Whisson[6]

[1]CSIRO Mineral Resources, 26 Dick Perry Avenue, Kensington, WA 6151, Australia

[2]The Institute for Geoscience Research (TIGeR), School of Earth and Planetary Sciences, Curtin University, GPO Box U1987, Perth, WA 6845, Australia

[3]Centre for Exploration Targeting, Curtin Node, School of Earth and Planetary Sciences, Curtin University, GPO Box U1987, Perth, WA 6845, Australia

[4]School of Geosciences, University of Aberdeen, Aberdeen AB24 3UE, UK

[5]CSIRO Energy, 26 Dick Perry Avenue, Kensington, WA 6151, Australia

[6]LabWest Minerals Analysis Pty Ltd, 28 Boulder Road, Malaga, WA 6090, Australia

Corresponding author:

Email address: David.fox1@csiro.au

Abstract

Reduction spheroids are small-scale, biogenic, redox-controlled, metal enrichments that occur within red beds globally. This study provides the first analysis of the compositionally unique reduction spheroids of the Tumblagooda Sandstone. The work aims to account for their composition and consequently improve existing models for reduction spheroids generally, which presently fail to account for the mineralogy of the Tumblagooda Sandstone reduction spheroids. Interstitial areas between detrital grains contained in the cores of these reduction spheroids are dominated by microplaty haematite, in addition to minor amounts of svanbergite, gorceixite, anatase, uraninite, monazite, and illite. The haematite-rich composition, along with an absence of base metal phases and the vanadiferous mica roscoelite, makes these reduction spheroids notable in comparison to other global reduction spheroid occurrences. Analyses of illite crystallinity provide values for samples of the Tumblagooda Sandstone host rock corresponding to heating temperatures of ~200°C. Consequently, while Tumblagooda Sandstone reduction spheroids formed via the typical metabolic processes of dissimilatory metal-reducing bacteria, the combination of a unique mineralogy and illite crystallinity analysis provides evidence of more complex late-stage heating and reoxidation. This has not previously been recognised in other reduction spheroids and therefore expands the existing model for reduction spheroid genesis by also considering the potential for late-stage alteration. As such, future reduction spheroid studies should consider the potential impact of post-formation modification, particularly where they are to be used as evidence of ancient microbial processes; such as in the search for early evidence of life in the geological record on Earth or other planets. Additionally, because of their potential for modification, reduction spheroids serve as a record of the redox

history of red beds and their study could provide insights into the evolution of redox conditions within a given red bed during its diagenesis. Finally, this paper also provides insights into the relatively understudied diagenetic history of the Tumblagooda Sandstone; supplying the first reliable and narrow constraints on its thermal history. This has important implications for the thermal history of the Carnarvon Basin and its petroleum prospectivity more broadly.

Introduction

Reduction spheroids are small-scale (<30 cm) metalliferous spheroidal features that occur in red terrestrial sedimentary rocks (red beds) and are defined by the presence of a dark mineralised core, with a surrounding pale haematite dissolution halo (Fig. 1). Interest in reduction spheroids primarily relates to their strong enrichment in redox-sensitive elements, including U, V, Au, Cu and Ag, among others (Hofmann, 1990a; Parnell et al., 2015a; Parnell et al., 2015b). Consequently, it has been proposed that reduction spheroids could be useful in (i) further understanding processes associated with low-temperature redox-controlled metal concentration in sedimentary rocks, such as in unconformity-related U deposits (Hofmann, 1999), and (ii) as a potential tool in exploration for regional metal anomalies (Parnell, 2017). The metabolic processes of dissimilatory metal-reducing bacteria (DMRB) consuming organic matter in the sediment are believed to be critical in the formation of reduction spheroids. Organic matter is used by these bacteria as an energy source and reductant to allow for the bacterially-mediated reductive precipitation of dissolved metals into the cores of reduction spheroids (Spinks et al., 2010; Spinks et al., 2014; Parnell et al., 2016). As such, reduction spheroids are believed to also be of use as a potential biomarker for recording the early colonisation of the terrestrial biosphere by metal-reducing bacteria and in the search for life in the Martian geological record (Spinks et al., 2010; Thompson et al., 2014; Parnell et al., 2015a; Spinks et al., in review).

Here, we investigate the reduction spheroids of the Tumblagooda Sandstone; an Ordovician-Silurian red bed that occurs through the base of the Southern Carnarvon Basin, cropping out in the area immediately surrounding the Kalbarri townsite in Western Australia (Hocking, 2000). It is notable that reduction spheroids at these localities are exceptionally abundant and compositionally unique relative to other red beds. Despite this, the reduction spheroids of the Tumblagooda Sandstone are completely unstudied. The aim of this paper is to provide the first study of the Tumblagooda Sandstone reduction spheroids in order to account for their unique mineralogy and, consequently, improve existing models for reduction spheroids generally as the existing models for reduction spheroid genesis do not adequately account for the mineralogy of the Tumblagooda Sandstone reduction spheroids. This holds key implications for understanding the processes that produce reduction spheroids broadly and is a particularly important consideration for future studies where reduction spheroids may be recognised as biomarkers of ancient DMRB in the early terrestrial biosphere on Earth and potentially Mars (Spinks et al., 2010; Thompson et al., 2014).

Geological Background

The Tumblagooda Sandstone (Kettanah et al., 2015) is an Ordovician–lower Silurian red bed that extends throughout most of the basal Southern Carnarvon Basin and portions of the northern Perth Basin of Western Australia (Fig. 2/3a) (Hocking, 1991). This formation is most prominent near Kalbarri, Western Australia and best exposed at its type section in the Murchison River gorge and along the coastal cliffs south of Kalbarri, ~600 km north of Perth (Fig. 3) (Hocking, 1991). The Tumblagooda Sandstone is inferred to be over 2000 m thick where it occurs through the Carnarvon Basin (Kettanah et al., 2015), and is observed to be 1210 m thick at its type section through the Murchison River Gorge (Hocking, 1991). The Silurian carbonate-rich Dirk Hartog Group is interpreted to conformably overlie the Tumblagooda Sandstone and provides conodont biostratigraphic age constraints (Iasky and Mory, 1999). The Tumblagooda Sandstone is of global palaeontological significance for its diverse and well preserved ichnofossils, which provide early evidence of a thriving ecosystem of terrestrial arthropods during the Silurian (Trewin and McNamara, 1995).

As the basal unit within the Southern Carnarvon Basin, the Tumblagooda Sandstone represents the earliest widespread sediment deposition following the initial formation of the Southern Carnarvon Basin in an epicratonic rift setting during the Late Ordovician (Hocking, 1991; Mory et al., 2003). The sediment source for the Tumblagooda Sandstone is poorly constrained, with provenance indicators historically providing ambiguous results. Reflecting this, the Yilgarn Craton, Albany-Fraser Orogen, Pinjarra Orogen, Capricorn Orogen, North Indian Orogen, East Africa, and Antarctica have all previously been proposed as potential sources based upon various analytical techniques. These techniques include detrital zircon U/Pb geochronology, analysis of heavy mineral assemblages, and petrographic analysis of textural and mineralogical characteristics of different portion of the Tumblagooda Sandstone (Hocking, 1991; Mory et al., 2003; Kettanah et al., 2015; Markwitz et al., 2017).

The Gascoyne Platform of the Southern Carnarvon Basin (Fig. 2) hosts the Tumblagooda Sandstone and is dominated by Ordovician to Devonian strata, with a thin cover of Cretaceous to Cenozoic sediments (Ghori, 1999). The deposition of the Tumblagooda Sandstone was followed by the Dirk Hartog Group carbonates and evaporites through the Late Ordovician and Silurian in a shallow-marine environment (Hocking et al., 1987; Hocking, 1991; Ghori, 1999). The deposition of the Dirk Hartog Formation was followed by deposition of carbonate and siliciclastic sediments following a short pause in deposition during the Early Devonian (Ghori, 1999; Mory et al., 2003). After an extended period of non-deposition until the Middle Devonian, a marine transgression was associated with the deposition of thick shallow marine to transitional strata throughout the Southern Carnarvon Basin during the Middle to Late Devonian (Hocking et al., 1987; Ghori, 1999; Iasky et al., 2003; Mory et al., 2003). This was followed by a significant depositional hiatus throughout most of the Gascoyne Platform until the Early Cretaceous, as the Gascoyne Platform was a positive topographic feature during this time (Iasky et al., 2003). This is proposed to be a consequence of uplift during the Middle Carboniferous due to the collision of Gondwana and Laurasia, rifting through the Middle Carboniferous to Permian activating several fault systems that diverted sediment to other depocentres, and non-deposition or erosion due to the rifting of India from Australia beginning in the Middle Jurassic (Iasky and Mory, 1999; Mory et al., 2003). The uppermost portion of the Southern Carnarvon Basin is dominated by Cretaceous to Cenozoic marine carbonates as a result of a widespread transgression during this period (Iasky and Mory, 1999; Mory et al., 2003).

Foundational work by Hocking (1991) recognised five stratigraphic facies associations (FA), designated FA1-FA5, reflecting broad-scale sedimentological variations within the Tumblagooda Sandstone. These facies associations and their stratigraphic relationships are summarised in Fig. 4 with the occurrence of reduction spheroids noted within the sequence. However, FA5 is not included due to its common omission from the literature, as discussed at the end of this section. This informal scheme has been adopted in subsequent works as the standard sub-divisions of the Tumblagooda Sandstone (Trewin and McNamara, 1995; Mory and Hocking, 2008).

FA1 is a red and white dominantly sandy, ~440 m thick sequence at the base of the Tumblagooda Sandstone that is largely devoid of bioturbation and interpreted to have been deposited in a large braided fluvial system (Hocking, 1991). The overlying FA2 is

200 m thick at the type section and is similarly dominated by red and white sandstone, though it is significantly more bioturbated (Hocking, 1991). This bioturbation has been referred to by Trewin (1993a) as the *'Heimdallia-Diplichnites Ichnofauna'*. Reduction spheroids were observed at the base of FA2, but were not logged in detail, as the coastal sections of the Tumblagooda Sandstone were the focus of this study. Hocking (1991; 2000; 2006) has consistently argued that FA2 was deposited within an intertidal environment. However, Trewin (1993b) and later, McNamara (2014), have suggested that FA2 was deposited in a mix of terrestrial fluvial and aeolian depositional environments. FA2 is sharply overlain by FA3, which is up to 260 m in thickness at the type section and is defined by a generally coarse-grained, poorly sorted, trough cross-bedded red sandstone that is observed to host abundant reduction spheroids (Hocking, 1991; Trewin and McNamara, 1995). The 'Gabba-Gabba Member', a laterally extensive pebbly marker bed, up to 1.2 m thick, occurs near the top of FA3 (Hocking, 1991). The occurrence of this bed also marks a significant increase in bioturbation, characterised as the '*Skolithos-Diplocraterion Ichnofauna*' (Trewin and McNamara, 1995). FA3 is up to 260 m at the type section and is generally interpreted to have been deposited in a high-energy braided-fluvial environment (Hocking, 1991; Trewin, 1993a; Trewin and McNamara, 1995; Hocking, 2000). The prevalence of bioturbation toward the top represents an increasing marine influence (Trewin and McNamara, 1995). FA3 can be observed to grade upwards into FA4 by the increasing presence of clay-rich beds of red siltstone (Hocking, 1991). With this considered, FA4 is exposed over up to 45 m at the type section and is generally defined by the presence of red oxidised and white reduced sandy siltstones and very fine to medium-grained sandstones, which may be intensely bioturbated by the '*Skolithos-Diplocraterion Ichnofauna*' (Hocking, 1991; Trewin,

1993a). These finer-grained lithologies are interpreted to indicate deposition in a lower energy deltaic environment, proximal to the fluvial environment of FA3 (Hocking, 2000). However, the abundant marine ichnofossils within FA4 could be accounted for by the reworking of wave-generated sandbars within a prograding fluvial system (Trewin, 1993a; Trewin and McNamara, 1995). Much like the underlying FA3, FA4 is also observed to contain reduction spheroids (Fig. 4); occurring densely through certain horizons. FA5 is isolated from the other facies associations, occurring to the east of the nearby Northampton Complex (Fig. 2/3a); a Proterozoic gneissic basement inlier of the Pinjarra Orogen (Fitzsimons, 2001). As such, FA5's stratigraphic relationship to the rest of the Tumblagooda Sandstone is unknown and it is commonly omitted from the literature (Trewin, 1993b; Trewin, 1993a; Trewin and McNamara, 1995; Trewin and Fallick, 2000; Kettanah et al., 2015). As a result of this and FA5's geographic isolation, it was not analysed in this study. Nonetheless, FA5 is dominated by coarse-grained red sandstones and conglomerates, and on this basis is interpreted to have been deposited in either a high-energy fluvial or alluvial system (Hocking, 1991). Broadly the climate at the time of deposition of this sequence (FA1-5) has been interpreted to be arid; as is characteristic of red beds generally (Walker, 1967).

Methods

Sample Collection and Preparation

Sampling of reduction spheroids for this study was undertaken through the sequence exposed at Red Bluff, Rainbow Valley, and Mushroom Rock (Fig. 3b/c). These localities correspond to FA3/FA4 and FA4, respectively (Hocking, 1991). As Red Bluff and Rainbow Valley provide excellent examples of FA3 and FA4, in this study FA3 will be herein informally referred to as the *Red Bluff unit (RBU)* and FA4 will be referred to as the *Rainbow Valley unit (RVU)*. Sampling at these localities was of in-situ reduction spheroids from several horizons within a sequence ~40 m thick over a strike length of ~2 km. Whilst an attempt was made to gather a representative collection of reduction spheroids from both localities, inevitably there was some degree of sampling bias toward average (~10 cm) and larger than average reduction spheroids. With this considered samples of a range of sizes (4.5-16 cm in diameter) were collected and analysed.

Eighteen reduction spheroids were prepared as polished blocks for non-destructive mineralogical and geochemical analyses, whilst twenty others were used for x-ray diffraction (XRD) analysis. Twenty-one samples of the host red-bed were also taken from the Rainbow Valley unit through to the base of Red Bluff unit. Three of these samples were then polished for non-destructive analyses; a red fluvial sandstone from the RBU (RBU-HR-29), a white reduced fluvial sandstone from the RBU (RBU-HR-23), and a red siltstone from the RVU (RVU-HR-17), whilst twenty-four samples were powdered for XRD. Additionally, clay separates were collected from two of the samples of Tumblagooda Sandstone that were also polished for petrographic analysis; one each from a sample of red sandstone from the RBU (RBU-HR-29) and white sandstone from the RBU (RBU-HR-23). These samples were lightly crushed, sieved, and clay-sized (<2 μm) particles were separated in deionised water.

Mineralogical and Geochemical Analysis

All the analyses performed in this study were conducted at the Commonwealth Scientific and Industrial Research Organisation (CSIRO) Advanced Resource Characterisation Facility at the Australian Resources Research Centre and at the John de Laeter Centre at Curtin University in Perth, Western Australia. XRD analyses were conducted using a Bruker D4 ENDEAVOUR (Bruker Corporation, Billerica, MA, USA) with a LynxEye Detector and a cobalt x-ray tube. Reduction spheroid cores and Tumblagooda Sandstone host rock sample powders were analysed in steel ring holders at 5-90° 2θ, 40 kV, and 35 mA. The clay separates from two host sandstone samples were analysed at 2-35° 2θ at 40 kV and 35 mA on a low-background Si slide in parallel and random orientations. These samples were also analysed for expanding clays through the addition of ethylene glycol to the slides and rescanning under the same parameters. The data were analysed using the Bruker DIFFRAC.EVA XRD software and machine performance were evaluated using corundum standards and referenced using known d-spacing of quartz within each sample.

All polished samples were investigated using reflected light microscopy with a Nikon LV100N POL (Nikon Instruments, Tokyo, Japan) to broadly define their microstructure, mineral composition, and textures. Additionally, elemental mapping was conducted using a Bruker M4 TORNADO (Bruker Corporation, Billerica, MA, USA) Micro-XRF mapper. Analyses were performed using a beam diameter and point spacing of 25 µm, with a dwell time between 5-10 ms. Further analysis of these samples was conducted using a Zeiss Ultra Plus (Carl Zeiss Microscopy GmbH, Jena, Germany) Field Emission Gun Scanning Electron Microscope (FEG-SEM), with energy-dispersive x-ray spectra collected using a Bruker XFlash 6 (Bruker Corporation, Billerica, MA, USA) energy-dispersive spectrometer (EDS). Typically, a working distance of ~6 mm was used; with an accelerating voltage of 5-20 kV and a beam current of 690 Pa. In addition, freshly broken samples were analysed using this SEM to observe the three-dimensional nature of the mineral associations within the reduction spheroids and host sandstone. The minerals were identified through semi-quantitative chemical analysis in combination with analysis of crystal morphologies and textures and then confirmed through XRD and electron backscatter diffraction analysis (EBSD). EBSD analysis was conducted on a Tescan Mira3 (TESCAN, Brno, Czech Republic) FEG-SEM fitted with an Oxford Instruments Aztec (Oxford Instruments plc, Abingdon, UK) acquisition system. These samples were coated with a thin carbon coat and analysed at a working distance of 18.5 mm, a stage tilt of 70°, and an accelerating voltage of 20 kV.

Computed Tomography Analysis

The samples were scanned in 3D by X-ray computed tomography (XCT) using a Siemens SOMATOM definition AS (Siemens AG, Berlin, Germany) medical scanner allowing the rapid 3D scanning of the reduction spheroids. The instrument was calibrated using air, water and a set of five in-house rock standards of known density that are suitable for mineral resources applications (2.7 to 4.3 g/cm^3). The energy of the beam was set-up to have maximal phase contrast between the detrital grains and interstitial metalliferous minerals. The voxel size (i.e. pixel in 3D) was set-up to 300 x 300 x 100 µm (~0.5 mm spatial resolution) to allow entire coverage of the samples. The CT data was processed and analysed using ThermoFisher Avizo 3D data visualisation software. The workflows used in this study are discussed further by Godel et al. (2006) and Godel (2013).

Results

Reduction Spheroid Occurrence and Appearance

Field Observations

At the most reduction spheroid-rich horizons within the coastal exposures of the Tumblagooda Sandstone, reduction spheroids occur in densities of approximately 15 per

m^2 (Fig. 1c) over a strike length of at least 2 km. The reduction spheroids present in the sand-rich RBU differ in appearance from those in the more clay-rich RVU (Fig. 1). The reduction spheroids of the RBU commonly contain slightly smaller, relative to their total volume, dark red-grey cores that are surrounded by reduction halos often containing concentrically zoned mineralised rings (Fig. 1a/b). By contrast, the reduction spheroids of the RVU typically contain larger dark grey cores within a beige reduction halo that commonly does not contain any outward concentric zoning (Fig. 1c/d). Throughout the Tumblagooda Sandstone, the reduction spheroids are commonly ovoid in shape, elongated parallel to bedding structures in the rock and generally range from 1-18 cm in diameter; with an average total diameter of ~10 cm and an average total core diameter of ~4 cm. Whilst the total reduction spheroid size is relatively consistent between the RBU and RVU, generally the reduction spheroids of the RVU tend to have slightly larger cores. It also worth noting that whilst reduction bands are occasionally observed to occur in association with reduction spheroids (Fig. 1d), reduction bands do not appear to have any specific genetic relationship to reduction spheroids as they are common throughout the Tumblagooda Sandstone, and other red beds globally; including where reduction spheroids are not observed. Instead the reduction bands most likely formed as a result of the migration of genetically unrelated reducing fluids during diagenesis (Parry et al., 2004).

Computed Tomography Analysis

The abundance of reduction spheroids facilitated the recovery of whole reduction spheroid samples, allowing the first ever CT imaging of the three-dimensional structure of a whole reduction spheroid to be conducted (Fig. 5). CT imaging demonstrates the three-dimensional nature of reduction spheroids, with a dense spheroidal core that is slightly oblate and has therefore been vertically shortened or horizontally elongated. Whilst all reduction spheroids are three-dimensional, it is relatively rare to observe a whole reduction spheroid as any reduction spheroid in an outcrop with an observable core must have been sufficiently eroded such that its internal core is visible. Consequently, being able to observe the three-dimensional, internal structure of a whole reduction spheroid is novel and can inform models for their formation and the relative influence of basinal fluid flow, sediment permeability, and compaction on their morphology and structure. Additional CT scan clips are also provided in the supporting information.

Mineralogy

X-Ray Diffraction

Reduction spheroid cores are all relatively similar in mineralogy and dominated by quartz and microcline. Most reduction spheroids also contain haematite and illite; however, two samples (RBU-RS-17 and RBU-RS-39) lack a haematite signature. It is also interesting to note that there is variation in the width of haematite peaks, with some samples (RBU-RS-1) containing noticeably broader peaks. This is possibly due to variation in haematite crystallinity across samples, with wider peaks indicative of less crystalline haematite (Schwertmann and Latham, 1986). The detection limits associated with powder XRD restricted the detailed identification of less abundant minerals. These less abundant mineral phases were characterised using microscopy techniques.

Analysis of the clay separates from the two samples (RBU-HR-23 and RBU-HR-29) of Tumblagooda Sandstone host rock revealed that the clay fraction of the rock is dominated by illite; as indicated by a sharp illite peak at 10 Å in the spectra. These samples are also characterised by the absence of the 12-15 Å peaks typical of smectite.

The absence of interstratified expanding clays, such as smectite, within the illite was further confirmed by the absence of shift of the 10 Å peak following addition of ethylene glycol to the samples (Srodon, 1980). Additional analysis of this illite, using randomly oriented samples, showed that it is composed of the lower temperature one-layer monoclinic (1M) polytype as it lacks any diagnostic two-layer monoclinic (2M) peaks (Grathoff and Moore, 1996). The absence of 2M polytype illite confirms an authigenic origin indicating that the illite formed due to heating during diagenesis (Weaver, 1958). The temperature of this heating can be estimated by measuring the crystallinity index of the illite in the samples using the illite peak width at half-height (Eberl and Velde, 1989). This analysis found an illite crystallinity of 0.451 for the sample of white reduced sandstone (RBU-HR-23), and 0.467 for the sample of red oxidised sandstone (RBU-HR-29). These values correspond to a heating temperature of ~200°C; accounting for the low smectite content within the illite in these samples, as this temperature of diagenesis corresponds to an interstratified smectite content of only ~5% within the illite (Merriman and Frey, 1999).

Optical and Scanning Electron Microscopy

Petrographic analysis of the 18 polished reduction spheroids confirmed detrital quartz and K-feldspar are the dominant minerals within spheroid cores. Quartz grains commonly show clear secondary quartz overgrowths and sutured grain contacts. K-feldspar grains range from fresh to pervasively weathered and are commonly replaced by interstitial illite. Intergranular porosity within the cores is filled with haematitic cement; occurring as a dense assemblage of coarse (10-200 µm) interstitial microplaty haematite crystals (MplH) (Fig. 6a/b) or fine haematite cement (crystals <10 µm) that is commonly intergrown with illite (Fig. 6c). Dark grey cores are intensely cemented by a coarse MplH that commonly fills fractures within weathered K-feldspar grains (Fig. 6a), which reduces both intergranular and intragranular porosity. Reddish cores tend to be cemented by a combination of fine haematite and illite (Fig. 6d). However, the majority of the reduction spheroid cores contain both coarse MplH and fine red haematite; resulting in variably grey and red portions.

Both the cores and surrounding reduction halos of the reduction spheroids are observed to contain low volumes of secondary anatase occurring as clusters between quartz and K-feldspar grains throughout the samples. These clusters are generally composed of aggregates of several anatase crystals and display a variety of textures; ranging from round clusters (50-200 μm) of needle-shaped crystals (<10 μm, Fig. 6e), trellis-like aggregates of acicular laths (Fig. 6f), to clusters of coarser (<100 μm) crystals that are equant in basal section and bladed along their long axis (Fig. 6g). The clusters of coarse anatase crystals are commonly surrounded by very fine (<1 μm) anatase aggregates (Fig. 6h). Additionally, the coarse anatase crystal often contain small (~1 μm) irregularly shaped uraninite inclusions (Fig. 7a).

Svanbergite ($SrAl_3(PO_4)(SO_4)(OH)_6$) and gorceixite ($BaAl_3(PO_4)(PO_3OH)(OH)_6$) are aluminium-phosphate-sulphate (APS) minerals that occur within both the spheroid cores and reduction halos. Svanbergite is commonly observed to occur as isolated inclusions within the MplH in the cores. It is also present as small cubic euhedral crystals (~4 μm) in the illite matrix, and as aggregates filling internal porosity in quartz and K-feldspar grains (Fig. 7b/c). Gorceixite occurs almost exclusively in association with svanbergite, forming rims surrounding svanbergite crystals (Fig. 7d). Illite occurs throughout the reduction spheroids as the only clay mineral and the dominant interstitial phase in the beige reduction halo of the reduction spheroids and commonly infills weathered voids within grains of K-feldspar. Small anhedral authigenic monazite crystals (<10 μm) occur as clusters of crystals commonly enveloped by quartz overgrowths or adhered to detrital grains (Fig. 7e).

For comparison with the reduction spheroids, three samples of Tumblagooda Sandstone host rock were petrographically analysed; a sample of red fluvial sandstone (RBU-HR-29), reduced white fluvial sandstone (RBU-HR-23), and red siltstone (RVU-HR-17). All three samples are dominated by detrital quartz and K-feldspar, with illite being the principal interstitial phase. The primary difference between the sandstone (RBU) and the siltstone (RVU) is that the latter contains significantly more illite and its detrital quartz and K-feldspar grains are finer. Gorceixite and svanbergite are rare within the three host rock samples, though they do occur. The distribution of these two APS minerals through the samples is similar to those observed in the reduction spheroids. Svanbergite forms aggregates of fine subhedral-euhedral crystals adhered to quartz grains or isolated crystals dispersed throughout the illite matrix, whereas gorceixite occurs solely as zoned rims around svanbergite grains. Although present, these APS minerals are much less abundant within the host Tumblagooda Sandstone compared to the reduction spheroids. Haematite in the red sandstone and siltstone is present as extremely fine needles (<1 μm) throughout the illite matrix, whereas it was not observed in the reduced white sandstone. Finally, unaltered detrital ilmenite grains (~100 μm) displaying magmatic exsolution textures (Fig. 7f) are observed within the red sandstone and siltstone. However, ilmenite was not observed within the reduction spheroids or the reduced white sandstone sample. The above information on the mineralogy and nature of the occurrence of these minerals in the host rock Tumblagooda Sandstone and reduction spheroids is summarised in Table 1.

Table 1 - Summary of minerals with abundance and nature of occurrence in host Tumblagooda Sandstone and reduction spheroids.

Mineral phase	Abundance and nature of occurrence
Quartz	Common. Primary. Dominant detrital mineral in host rock and throughout reduction spheroids.
K-feldspar	Common. Primary. Abundant detrital mineral in host rock and throughout reduction spheroids.
Heavy minerals	Common. Primary. Detrital zircon, monazite, ilmenite, and rutile common in red host sandstone. Detrital ilmenite, rutile, and monazite are rare in white sandstone and reduction spheroids.
Svanbergite	Common. Authigenic. Occurs throughout reduction spheroids in aggregates of cubic crystals filling interstitial space.
Gorceixite	Common. Authigenic. Occurs exclusively rimming svanbergite crystals.
Uraninite	Trace. Authigenic. Occurs exclusively as inclusions within anatase throughout spheroids.
Anatase	Trace. Authigenic. Occurs as clusters of acicular anatase needles in interstitial space in reduction spheroid cores with very fine (<1 μm) surrounding aggregates.
Monazite	Trace. Authigenic. Occurs as clusters of crystals (<10 μm) commonly adhered to detrital quartz grains in reduction spheroid cores.
Microplaty haematite (MplH)	Common. Authigenic. Dominates interstitial space through majority of reduction spheroid cores.
Illite	Common. Authigenic. Dominates interstitial space in reduction spheroid halos and host rock, also occurs through less dense reddish cores.
Fine haematite	Common, occurs in association with MplH in reddish cores and commonly intergrown with illite.

Geochemistry

X-Ray Fluorescence Mapping

Cores of reduction spheroids contain abundant Fe (haematite), mainly as an interstitial component or surrounding quartz grains (Fig. 8). Within these cores, the strong Fe enrichment reflects the predominance of MplH within the reduction spheroid cores. Though Fe is observed within the host red sandstone surrounding the reduction spheroids, it is significantly more abundant in the cores of the reduction spheroids. By contrast, Fe is absent in the pale reduction halos, which are dominated by Si (quartz) and K (K-feldspar). In some samples (RBU-RS-8, 50) weathered fractures in K-feldspar grains are clearly penetrated by Fe (Fig. 6a/8b). Additionally, the concentric rings that occur in some reduction spheroid samples (RBU-RS-11, 36, 43, and RVU-RS-55) are similarly enriched in Fe but tend to be more sparsely mineralised than the cores; with lower Fe-enrichment.

Thin bands of Ti-bearing phases occur consistently (RBU-RS-6, 50; Fig. 8a/b) throughout several reduction spheroid samples. These Ti-bearing phases most likely correspond to the previously discussed authigenic anatase. The Ti distribution follows similarly oriented straight lines running parallel or sub-parallel to one another and to the prevailing sedimentary fabric. These bands cross-cut the central mineralised spheroid cores (RVU-RS-48 and RBU-RS-50) as well as the reduction halos. Although the Fe-rich core is cross-cut by these thin bands of Ti, the Ti-enrichment is generally discontinuous across it. In some cases (RBU-RS-7 and RVU-RS-55) the Fe-enrichment also appears to disperse from the core and concentric rings along the sedimentary fabric (Fig. 8c/d/e).

Discussion

Comparisons with Typical Reduction Spheroids

Morphology

The Tumblagooda Sandstone reduction spheroids resemble reduction spheroids from other red beds around the world in several aspects. For instance, the slight horizontal elongation of reduction spheroids in the Tumblagooda Sandstone (Fig. 5) and in exposed reduction spheroids in outcrop, mirrors that observed by Mykura and Hampton (1984); Hofmann (1990b); Lines et al. (1995); Spinks et al. (2010). This can be explained by the formation of the reduction spheroids prior to sediment compaction or due to improved fluid diffusion along sedimentary fabrics parallel to bedding structures (Hofmann, 1990b; Spinks et al., 2010). The latter explanation may account for the horizontal diffusion of mineralisation out from the cores of some of the Tumblagooda Sandstone reduction spheroids and their elongation parallel to sedimentary structures (i.e. cross-bedding) (Fig. 8c/d/e). Cumulatively, these observations imply that the improved permeability along pre-existing non-horizontal sedimentary structures and the potential for basinal fluid migration along these structures during reduction spheroid formation impart a significant control on the morphology of a given reduction spheroid. This information contradicts previous interpretations that reduction spheroids are oblate due to vertical shortening as a result of sediment compaction (Spinks et al., 2010).

The concentric rings present in reduction spheroids from the RBU also resemble the zonation in reduction spheroids observed by Carter (1931); Hofmann (1990b); Lines et al. (1995); Milodowski et al. (2002); Spinks et al. (2014), which also exhibit a mineralogy consistent with the central core. An explanation for the formation of these concentric rings has not been offered. However, similar structures exist within carbonate concretions; which are similarly believed to form through the consumption of organic matter by sub-surface microbial communities (Marshall and Pirrie, 2013; Plet et al., 2016). Within carbonate concretions, this concentric zoning is typically interpreted to be a growth feature related to the outward growth of concretions from a central nucleus during discrete stages (Mozley, 1996; Marshall and Pirrie, 2013). Similarly, the concentric rings present in the Tumblagooda Sandstone reduction spheroids, and reduction spheroids from other localities, could reflect progressive changes in reduction spheroid forming processes and condition, including the intensity of microbial activity; availability of metals; and pore-water chemistry.

Despite strong similarities between the spheroids observed here and in previous studies, a few discrepancies were also observed. Variations in terms of appearance and morphology of the reduction spheroids were observed within the Tumblagooda Sandstone, particularly between those hosted in the coarse fluvial sandstone of the RBU and the overlying siltstone of the RVU. Specifically, the reduction spheroids that occur within the RVU contain larger cores that are more densely mineralised with MplH, and consequently display a darker grey colour (Fig. 1). This finding contradicts observations made by Lines et al. (1995) on reduction spheroids from The Hopewell Group of New Brunswick, where coarser grained units hosted larger reduction spheroids with correspondingly larger cores. This relationship between grain size and reduction spheroid size was accounted for by the increased porosity and permeability associated with coarser grained sediment. However, the contradictory nature of the findings of the present study and those of Lines et al. (1995), suggest that in the studied cases the effect of grain size on porosity and permeability does not impart a critical control on the size of reduction spheroids generally. In the present study, the larger cores within the finer grained clay-bearing siltstones of the RVU may be explained by the greater concentration of trace metals within these units available for incorporation into reduction spheroids' cores, when compared with the more quartz and feldspar-rich sandstones in the RBU (Supp. info.; Pettijohn, 1963).

Mineralogy and Geochemistry

Compositionally, the reduction spheroids of the Tumblagooda Sandstone are unique in comparison to reduction spheroids previously reported from other localities. This is because their cores are enriched in Fe due to their haematite-dominated mineralogy. Haematite is an oxidised Fe phase, yet reduction spheroids form via the reductive concentration of dissolved metals through the metabolic processes of DMRB (Spinks et al., 2010). Therefore, haematite is a particularly uncommon constituent of typical reduction spheroids (Hofmann, 1991). One would expect that magnetite, a reduced Fe phase that is observed to form via the biomineralising activity of DMRB (Lovley, 1991; Lovley, 1993; Lovley et al., 2004), could be commonly observed in reduction spheroids, yet magnetite is also relatively rare in reduction spheroids. Overall, reduction spheroids are most often depleted in Fe in comparison to their red host sandstones (Hofmann, 1990a; Hofmann, 1990b; Hofmann, 1991). This makes the abundance of haematite, and the related Fe-enrichment, within the Tumblagooda Sandstone reduction spheroids' cores particularly exceptional. In addition, the presence of svanbergite, gorceixite, authigenic anatase, and authigenic monazite within the Tumblagooda Sandstone reduction spheroids is also unique as none of these minerals have previously been observed in reduction spheroids. These mineral phases are, however, relatively minor in abundance in comparison to the MplH cement in the reduction spheroids and the observation of these unique mineral phases may simply reflect the fact that the analytical techniques used in previous studies may not have allowed for the identification of relatively low abundance and fine-grained minerals such as svanbergite, gorceixite, and anatase.

Roscoelite ($K(Al,V,Mg,Fe)_2(Si,Al)_4O_{10}(OH)_2$) is a vanadiferous mica that is common in previously studied reduction spheroids; particularly those from Devonian red beds (Hofmann, 1991; Van Panhuys-Sigler et al., 1996; Spinks et al., 2010; Spinks et al., 2014; Parnell et al., 2015b), but is conspicuously absent from the Tumblagooda Sandstone reduction spheroids. Despite their predominance within reduction spheroids from other localities (Hofmann, 1990a; Hofmann, 1990b; Hofmann, 1991), reduced mineral phases are uncommon within the Tumblagooda Sandstone reduction spheroids, except for minor amounts of uraninite (Fig. 7a). Finally, it is noteworthy that, unlike reduction spheroids from other localities (Harrison, 1975; Harrison et al., 1983; Hofmann, 1990b; Spinks et al., 2014), reduction spheroids of the Tumblagooda Sandstone contain no evidence of even trace quantities of any base metal phases.

Record of Diagenetic Conditions

Evidence of an acidic microenvironment during reduction spheroid formation

Reductive activity of DMRB during early diagenesis within the reduction spheroids would have created a microenvironment by controlling the redox conditions at the µm-scale. This would have also generated geochemical conditions conducive to the authigenic formation of svanbergite and anatase within the Tumblagooda Sandstone. Authigenic anatase is interpreted to be a product of the local mobilisation of Ti from the unaltered primary titaniferous minerals that are observed within the red Tumblagooda Sandstone host rock (ilmenite, Fig. 7f), but are no longer observed within the reduction spheroids. Additionally, the mobilisation of Ti from primary ilmenite and reprecipitation elsewhere within the reduction spheroids as anatase may account for discontinuity of Ti-rich bands across the Fe-rich cores of the reduction spheroids within the XRF map of RBU-RS-50 (Fig. 8b). These Ti-rich bands represent horizons of detrital titaniferous heavy minerals. Due to the immobility of Ti (Schulz et al., 2016), the anatase banding is believed to be inherited from the primary distribution of the ilmenite from which it was derived. However, the extreme immobility of Ti necessitates strongly acidic conditions (pH <2) to mobilise it from primary ilmenite (Sugitani et al., 1996). Therefore, the Ti discontinuity across the centre of the reduction spheroid cores is due to the fact that this was the most intensely reducing and acidic portion of Tumblagooda Sandstone reduction spheroids and, consequently, was the only portion where conditions were sufficiently acidic to mobilise Ti. Spinks et al. (in review) have proposed that humic acids would be necessary for reduction spheroid genesis as a chelator to locally mobilise metals and allow reduction spheroid formation through microbial activity. The presence of humic acids could also have provided the acidic conditions necessary to locally mobilise Ti within reduction spheroid cores. Humic acids are also commonly proposed as a chelator in the wider context of microbial metal reduction in nature, particularly because of their relative abundance in soils and sediments (Lovley et al., 1996; Lovley et al., 1998). These humic acids would have been derived from the microbial degradation of the detrital organic matter that acts as the reducing agent and energy source in reduction spheroid genesis. Further evidence of these intensely acidic conditions is provided by the presence of the svanbergite that is particularly common throughout the reduction spheroids. Svanbergite, and other APS minerals, are typically associated with strongly acidic migrating fluids, when observed in sediments (Dill, 2001; Benito et al., 2005; Galán-Abellán et al., 2013; Salama, 2014).

Under reducing conditions, svanbergite becomes stable only under increasingly acidic conditions (Gaboreau et al., 2005).

Reduction spheroid reoxidation

Abundant haematite throughout the cores of the Tumblagooda Sandstone reduction spheroids is most likely a product of a later stage reoxidation, following the cessation of reduction by DMRB and exhaustion of the available organic matter in the reduction spheroids. As such, the precursor of the haematite in these reduction spheroids was probably fine-grained biogenic magnetite; a common product of the biomineralising metabolic processes of DMRB (Lovley, 1991; Lovley et al., 2004). Once reducing conditions had ceased within the reduction spheroids, this biogenic magnetite may have been oxidised, as a result of exposure to oxidising conditions within the red bed. Whether this is related to the background oxidising conditions of the red bed or exposure to an oxidising fluid during diagenesis is difficult to determine. However, the prior explanation fails to account for why reduction spheroids in other red beds have not similarly been reoxidised. Therefore, it is interpreted here that the Tumblagooda Sandstone reduction spheroids were reoxidised due to exposure to oxidising high-temperature basinal fluids during diagenesis. The lack of comparable reoxidation or other diagenetic overprinting in reduction spheroids within other red beds may be attributable to the relatively extensive deep burial and diagenesis of the Tumblagooda Sandstone, which is discussed in the next section. This contrasts with roscoelite-bearing reduction spheroids from various localities that are interpreted to have been exposed to maximum burial temperatures of <150 °C or present evidence of limited basinal fluid-rock interaction (Hanly et al., 2003; Parnell et al., 2015b; Parnell et al., 2016; Parnell et al., 2018). Additionally, Fe-enrichment and the formation of Fe-oxide phases must have occurred during diagenesis; after the weathering of K-feldspar grains. This is evidenced by the penetration of MplH and Fe-enrichment through weathered fractures in these K-feldspar grains (Fig. 6a/8b). This later stage of reoxidation may account for the absence of minerals such as roscoelite or the other reduced phases that are characteristic of reduction spheroids from other localities but are not observed within the Tumblagooda Sandstone. It is likely that other reduced phases formed during active reduction within the reduction spheroids, but the later oxidising processes that formed the MplH currently present in the reduction spheroid cores would have destabilised and altered such minerals. This is with the exception of uraninite, which forms exclusively under reducing conditions (Janeczek and Ewing, 1992). It is proposed that uraninite is preserved within these reduction spheroids due to its occurrence as inclusions within larger grains of authigenic anatase, which may have protected it from exposure to oxidising conditions.

Reduction spheroid heating

Oxidation of reduction spheroids would have been synchronous with and followed by the progressive burial of the host red bed. Quartz overgrowth cement is ubiquitous in sandstones globally (McBride, 1989), and well developed quartz overgrowths are present within the reduction spheroids just as they are within the host Tumblagooda Sandstone. Inclusions of early diagenetic minerals are present within these quartz overgrowths whilst none of the hypothesised reduced phases have been preserved in the overgrowths. This implies that they were altered prior to the host rock being buried, leading to the formation of quartz overgrowths. Whilst quartz cementation is generally proposed to form at temperatures between 60-100 °C (McBride, 1989), the majority of quartz cementation occurs at temperatures greater than 90-100 °C. Previous work on the

Tumblagooda Sandstone proposed that the finalisation of its quartz cementation took place at temperatures of >100 °C and depths of >3 km, in the presence of meteoric fluids (Bjorlykke and Egeberg, 1993; Trewin and Fallick, 2000). Within the Tumblagooda Sandstone reduction spheroids, the majority of quartz cementation appears to have taken place prior to the development of MplH and illite.

Microplaty haematite in sedimentary rocks exclusively forms as a product of the heating and recrystallisation of fine grained and amorphous precursor Fe-bearing oxides and hydroxides. Additionally, estimates of the temperature at which MplH begins to form typically range from 80-100 °C and up to 150 °C (Catling and Moore, 2003; Morris, 2012). The oxidation of fine-grained biogenic magnetite within reduction spheroid cores would have provided a suitable fine-grained Fe-oxide precursor to MplH as the dominant mineral within reduction spheroids. This fine-grained oxidised Fe oxide precursor could then have been thermally coarsened to MplH during burial, with the potential driver of both this reoxidation and thermal coarsening being high temperature oxidising basinal fluids. It is interpreted that the majority of the MplH formed after the majority of the quartz cementation had occurred as, texturally, the MplH appears to postdate quartz overgrowths in the spheroids. Therefore, because the majority of the quartz cementation in the Tumblagooda Sandstone took place at >100 °C, the MplH is similarly interpreted to have formed at >100 °C, following further burial. Considering this, the presence of fine grained red haematite within some reduction spheroid cores is interpreted to have formed at cooler temperatures after the formation of the MplH; possibly by the leaching and reprecipitation of Fe from MplH by relatively cool fluids (<100 °C) after the exhumation and resultant cooling of the Tumblagooda Sandstone (Morris, 2003). This information and the paragenetic sequence of mineral formation in the genesis of the Tumblagooda Sandstone reduction spheroids are summarised in Fig. 9.

Further evidence of the heating of the Tumblagooda Sandstone reduction spheroids is provided by authigenic illite, which most likely formed as a product of the illitisation of smectite due to burial-related heating (Trewin and Fallick, 2000; Worden and Morad, 2003). Illitisation of smectite is a gradual process that begins at diagenetic temperatures as low as ~40 °C (Eberl, 1993), though this depends on several factors, including time and K-availability (Bjorlykke, 1998). Nonetheless, the illite crystallinity results for the host sandstone consistently record peak diagenetic temperatures of ~200 °C; indicating authigenic illite formation was a process that continued through deep burial. The presence of this highly crystalline illite with low smectite content, along with the aforementioned MplH and quartz cementation point unequivocally to the deep burial and heating of these reduction spheroids. This is also supported by geochemical and petrographic analysis that suggested the dolomitisation and formation of anhydrite cements within the overlying Dirk Hartog Group occurred at relatively high temperatures during burial (El-Tabakh et al., 2004).

The thermal history of the Tumblagooda Sandstone is not particularly well constrained; with apatite fission track analysis constraining its maximum palaeotemperature to >110 °C (Ghori et al., 2005). Theoretical basin modelling of the ‘Quail 1’ drill hole from the Merlinleigh sub-basin and the ‘Coburn 1’ drill hole from the Gascoyne Platform of the Southern Carnarvon Basin constrained the peak burial temperature of horizons of the Tumblagooda Sandstone to ~110 °C and ~220 °C, respectively (Ghori, 1999). This modelling was based largely on the extrapolation of thermal maturity data from overlying units and bottom-hole temperature measurements; leading to a relatively imprecise estimate of palaeotemperature (Deming, 1989). Further, palaeotemperature estimates of portions of the Tumblagooda Sandstone present in the Merlinleigh Sub-basin are arguably not applicable to the Tumblagooda Sandstone in Kalbarri, due to their presence in a different sub-basin. This study therefore provides valuable constraints on the thermal history of the Tumblagooda Sandstone; supporting previous assertions regarding the exposure of portions of the Tumblagooda Sandstone to temperatures of ~200 °C and providing the first narrow, and relatively reliable, constraints on the peak heating of the Tumblagooda Sandstone.

Research Significance and Implications

This work re-evaluates existing genetic models for reduction spheroids by considering modifying processes relevant subsequent to the cessation of microbial activity. Whereas existing models for reduction spheroid genesis assume formation is complete upon the exhaustion of organic matter within their cores and the corresponding cessation of active bacterial metal reduction (Spinks et al., 2010; Parnell et al., 2015b), this work shows for the first time that deep basinal diagenetic processes can affect the composition of reduction spheroids long after their original formation. Not only is this important in understanding the genesis of reduction spheroids generally as it adds a new component to the existing reduction spheroid genetic model, but it has significant implications for studies that utilise reduction spheroids. This is particularly key in studies where reduction spheroids are used as biomarkers for DMRB in terrestrial environments, based upon their enrichment in redox-sensitive metals and reduced authigenic mineral phases (Spinks et al., 2010; Parnell et al., 2015a). Particularly pertinent examples of such studies include those where reduction spheroids are used as biomarkers for life's earliest colonisation of the terrestrial environment through DMRB or in the search for signs of primitive extraterrestrial life, such as in the case of the Mars 2020 rover (Weber et al., 2006; Spinks et al., 2010; Thompson et al., 2014; Parnell et al., 2015a). This is especially pertinent due to the growing broad interest in Martian geology, particularly as it relates to the search for evidence of ancient life in the Martian geological record. This work is made even more relevant by the noted plausibility of bacterial metal reduction as a metabolic process for Martian life (Weber et al., 2006). If mineralogical analysis of any reduction spheroids discovered in studies searching for evidence of DMRB were to observe oxidised mineral phases within reduction spheroids, they may misinterpret that such features are not biomarkers for DMRB when in fact their original reduced mineral composition has simply been altered. This is similarly an important consideration where reduction spheroids would potentially be used in a mineral exploration setting, where their initial composition would potentially be used as a pathfinder for regional metal anomalies (Spinks et al., 2014; Parnell et al., 2015b; Parnell et al., 2016).

It is proposed that, based on the findings of this study, the potential for reduction spheroid alteration could provide insights into the diagenetic conditions experienced by their host formations during burial. This has particular potential in quartz-dominated sediments, which may not record diagenetic processes with any fidelity due to their particularly non-reactive composition. The MplH-rich mineralogy present in the Tumblagooda Sandstone reduction spheroids suggests exposure to elevated diagenetic temperatures (>100 °C) in the presence of oxidising basinal fluids. This compliments evidence from illite crystallinity analysis and the presence of very well-developed quartz cementation to suggest that the Tumblagooda Sandstone reached a peak burial temperature ~200 °C. Whilst of more regional significance, these data provide the first tight constraints on the poorly constrained diagenetic history of the Tumblagooda Sandstone and may have broader implications for the development of the Western Australian margin. This is due to the Tumblagooda Sandstone's position as the basal unit in the Southern Carnarvon and Perth Basins and consequent exposure to several major rifting events during the evolution of these basins (Ghori, 1999; Mory et al., 2003; Markwitz et al., 2017).

Conclusions

This study provides the first analysis of the abundant reduction spheroids that occur through the Tumblagooda Sandstone; indicating that they are noteworthy for their atypical composition. Geochemical and petrographic analyses reveal that the reduction spheroids' cores are strongly enriched in Fe; with the dominant authigenic mineral being microplaty haematite occurring between grains of detrital quartz and K-feldspar. However, authigenic anatase, uraninite, svanbergite, gorceixite, and monazite are also observed as minor phases throughout the reduction spheroid cores. Unlike reduction spheroids from other localities, no base metal phases or roscoelite are observed within Tumblagooda Sandstone spheroid cores. The occurrence of oxidised microplaty haematite throughout all of the reduction spheroids' cores is both unique and difficult to reconcile with a model for reduction spheroid genesis via DMRB. As such, it is proposed that the reduction spheroids of the Tumblagooda Sandstone were oxidised during diagenesis, subsequent to their initial formation, with the microplaty haematite in the reduction spheroids having formed through the reoxidation and heating of fine-grained biogenic magnetite. During this process it is likely that other reduced phases, such as roscoelite or base metal phases, which are characteristic of reduction spheroids from other localities, were destroyed. The potential for reduction spheroid reoxidation post-formation has not previously been considered in other studies and resultantly provides new insights into the genesis of reduction spheroids more broadly. Consequently, it is important that future reduction spheroid studies consider the currently unrecognised potential for the pervasive post-formation alteration of reduction spheroids. This is important to consider when attempting to utilise reduction spheroids as evidence of DMRB based on their reduced mineralogy. This is a key consideration in studies where reduction spheroids are used as mineralogical record of the metabolic processes of ancient DMRB; for example, in the search for evidence of the early colonisation of the terrestrial biosphere or signs of ancient life on Mars. However, it is proposed here that due to their potential for post-formation alteration, reduction spheroids could also provide a unique record of the evolution of redox conditions in red beds through detailed mineralogical analysis. More locally, this study also provides insights into the understudied diagenesis of the Tumblagooda Sandstone, including the first reliable and narrow constraints on its thermal history. As the Tumblagooda Sandstone is the basal unit of the Perth and Carnarvon basins these new constraints on burial and broader diagenesis may have important implications for understanding the evolution of these basins.

References

Benito, M.I., De la Horra, R., Barrenechea, J.F., López-Gómez, J., Rodas, M., Alonso-Azcárate, J., Arche, A. and Luque, J. (2005) Late Permian continental sediments in the SE Iberian Ranges, eastern Spain: Petrological and mineralogical characteristics and palaeoenvironmental significance. *Palaeogeography, Palaeoclimatology, Palaeoecology*, **229,** 24-39.

Bjorlykke, K. (1998) Clay mineral diagenesis in sedimentary basins - a key to the prediction of rock properties. Examples from the North Sea Basin. *Clay Minerals*, **33,** 15-34.

Bjorlykke, K. and Egeberg, P.K. (1993) Quartz Cementation in Sedimentary Basins. *The American Association of Petroleum Geologists Bulletin*, **77,** 1538-1548.

Carter, G.E.L. (1931) An occurrence of vanadiferous nodules in the Permian beds of South Devon. *Mineralogical Magazine***,** 609-613.

Catling, D.C. and Moore, J.M. (2003) The nature of coarse-grained crystalline hematite and its implications for the early environment of Mars. *Icarus*, **165,** 277-300.

Deming, D. (1989) Application of bottom-hole temperature corrections in geothermal studies. *Geothermics*, **18,** 775-786.

Dill, H.G. (2001) The geology of aluminium phosphates and sulphates of the alunite group minerals: a review. *Earth-Science Reviews*, **53,** 35-93.

Eberl, D.D. (1993) Three Zones for Illite Formation during Burial Diagenesis and Metamorphism. *Clays and Clay Minerals*, **41,** 26-37.

Eberl, D.D. and Velde, B. (1989) Beyond The Kubler Index. *Clay Minerals*, **24,** 571-577.

El-Tabakh, M., Mory, A.J., Schreiber, B.C. and Yasin, R. (2004) Anhydrite cements after dolomitization of shallow marine Silurian carbonates of the Gascoyne Platform, Southern Carnarvon Basin, Western Australia. *Sedimentary Geology*, **164,** 75-87.

Fitzsimons, I.C.W. (2001) The Neoproterozoic evolution of Australia's western margin. In: *From Basins to Mountains: Rodinia at the turn of the Century*, **65**. Geological Society of Australia, Abstracts, Perth, Western Australia.

Gaboreau, S., Beaufort, D., Vieillard, P. and Partier, P. (2005) Aluminum phosphate–sulfate minerals associated with Proterozoic unconformity-type uranium deposits in the East Alligator River uranium field, Northern Territories, Australia. *The Canadian Mineralogist*, **43,** 813-827.

Galán-Abellán, A.B., Barrenechea, J.F., Benito, M.I., De la Horra, R., Luque, J., Alonso-Azcárate, J., Arche, A., López-Gómez, J. and Lago, M. (2013) Palaeoenvironmental implications of aluminium phosphate-sulphate minerals in Early–Middle Triassic continental sediments, SE Iberian Range (Spain). *Sedimentary Geology*, **289,** 169-181.

Ghori, K.A.R. 1999. Silurian–Devonian petroleum source-rock potential and thermal history, Carnarvon Basin, Western Australia, Geological Survey of Western Australia, Perth, Western Australia.

Ghori, K.A.R., Mory, A.J. and Iasky, R.P. (2005) Modeling petroleum generationin the Paleozoic of the Carnarvon Basin, Western Australia: Implications for prospectivity. *AAPG Bulletin*, **89,** 27-40.

Godel, B. (2013) High resolution X-ray computed tomography and its application to ore deposits: from data acquisition to quantitative three-dimensional measurements with case studies from Ni-Cu-PGE deposits. *Economic Geology*, **108,** 2005-2020.

Godel, B., Barnes, S.J. and Maier, W.D. (2006) 3-D distribution of sulphide minerals in the Merensky Reef (Bushveld Complex, South Africa) and the JM Reef (Stillwater Complex, USA) and their relationship to microstructures using X-ray computed tomography. *Journal of Petrology*, **47,** 1853-1872.

Grathoff, G.H. and Moore, D.M. (1996) Illite Polytype Quantificationg Using Wildfire© Calculated X-ray Diffraction Patterns. *Clays and Clay Minerals*, **44,** 835-842.

Hanly, A.J., Geboy, N.J., Hiatt, E.E. and Kyser, K. (2003) Diagenesis, stratigraphy, paleohydrology, and lead isotope study of the Proterozoic Sibley Group, Western Ontario. In: *Geological Society of America Annual Meeting*, **35**, pp. 234. Geological Society of America Seattle.

Harrison, R.K. 1975. Concretionary Concentrations of the Rarer Elements in Permo-Triassic Red Beds of South-west England, Institute of Geological Sciences, London.

Harrison, R.K., Old, R.A., Styles, M.T. and Young, B.R. 1983. Coffinite in nodules from the Mercia Mudstone Group (Triassic) of the IGS Knowle Borehole, West Midlands, Institute of Geological Sciences, London.

Hocking, R.M. 1991. The Silurian Tumblagooda Sandstone, Western Australia, Geological Survey of Western Australia, Perth, Western Australia.

Hocking, R.M. 2000. Geology of the Southern Carnarvon Basin, Western Australia — a field guide, Geological Survey of Western Australia, Perth, Western Australia.

Hocking, R.M. 2006. Geology of the Kalbarri area — a field guide, Geological Survey of Western Australia, Perth, Western Australia.

Hocking, R.M., Moors, H.T. and Van De Graaff, W.J.E. 1987. Geology of the Carnarvon Basin Western Australia, Geological Survey of Western Australia, Perth.

Hofmann, B.A. 1990a. Reduction spheres in hematitic rocks from northern Switzerland: implications for the mobility of some rare elements, National Cooperative for the Disposal of Radioactive Waste, Wettingen, Switzerland.

Hofmann, B.A. (1990b) Reduction spheroids from northern Switzerland: Mineralogy, geochemistry and genetic models. *Chemical Geology*, **81,** 55-81.

Hofmann, B.A. (1991) Mineralogy and Geochemistry of Reduction Spheroids in Red Beds. *Mineralogy and Petrology*, **44,** 107-124.

Hofmann, B.A. 1999. Geochemistry of Natural Redox Fronts - A Review, National Cooperative for the Disposal of Radioactive Waste, Wettingen, Switzerland.

Iasky, R.P., D'Ercole, C., Ghori, K.A.R., Mory, A.J. and Lockwood, A.M. 2003. Structure and petroleum prospectivity of the Gascoyne Platform, Western Australia, Western Australia Geological Survey, Perth.

Iasky, R.P. and Mory, A.J. 1999. Geology of the Gascoyne Platform Southern Carnarvon Basin Western Australia, Geological Survey of Western Australia, Perth, Western Australia.

Janeczek, J. and Ewing, R.C. (1992) Dissolution and alteration of uraninite under reducing conditions. *Journal of Nuclear Materials*, **190,** 157-173.

Kettanah, Y.A., Mory, A.J., Wach, G.D. and Wingate, M.T.D. (2015) Provenance of the Ordovician-lower Silurian Tumblagooda Sandstone, Western Australia. *Australian Journal of Earth Sciences*, **62,** 817-830.

Lines, A.W., Parnell, J. and Mossman, D.J. (1995) Reduction spheroids from the Upper Carboniferous Hopewell Group, Dorchester Cape, New Brunswick: notes on geochemistry, mineralogy and genesis. *Atlantic Geology***,** 159-172.

Lovley, D.R. (1991) Magnetite Formation During Microbial Dissimilatory Iron Reduction. In: *Iron Biominerals* (Eds R.B. Frankel and R.P. Blakemore), pp. 151-166. Springer Science, New York, USA.

Lovley, D.R. (1993) Dissimilatory Metal Reduction. *Annual Review of Microbiology***,** 263-290.

Lovley, D.R., Coates, J.D., Blunt-Harris, E.L., Phillips, E.J.P. and Woodward, J.C. (1996) Humic substances as electron acceptors for microbial respiration. *Nature*, **382,** 445-448.

Lovley, D.R., Fraga, J.L., Blunt-Harris, E.L., Hayes, L.A., Phillips, E.J.P. and Coates, J.D. (1998) Humic Substances as a Mediator for Microbially Catalyzed Metal Reduction. *Acta Hydrochimica et Hydrobiologica*, **26,** 152-157.

Lovley, D.R., Holmes, D.E. and Nevin, K.P. (2004) Dissimilatory Fe(III) and Mn(IV) Reduction. *Advances in Microbial Physiology*, **49,** 219-286.

Markwitz, V., Kirkland, C.L., Wyrwoll, K.H., Hancock, E.A., Evans, N.J. and Lu, Y. (2017) Variations in Zircon Provenance Constrain Age and Geometry of an Early Paleozoic Rift in the Pinjarra Orogen, East Gondwana. *Tectonics*, **36,** 2477-2496.

Marshall, J.D. and Pirrie, D. (2013) Carbonate concretions-explained. *Geology Today*, **29,** 53-62.

Martin, D.M., Johnson, S.P., Riganti, A. and Hogen-Esch, J. (2016) 1:500 000 State interpreted bedrock geology of Western Australia (Ed S.R. White). Geological Survey of Western Australia, Perth.

McBride, E.F. (1989) Quartz Cement in Sandstone: A Review. *Earth-Science Reviews*, **26,** 69-112.

McNamara, K.J. (2014) First Footfall. In: *Geoscientist*, pp. 10-15. Geological Society of London, London, UK.

Merriman, R.J. and Frey, M. (1999) Patterns of Very Low-Grade Metamorphism in Metapelitic Rocks. In: *Low-Grade Metamorphism* (Eds M. Frey and D. Robinson), pp. 61-107. Blackwell Publishing Ltd., Oxford, UK.

Milodowski, A.E., Styles, M.T., Horstwood, M.S.A. and Kemp, S.J. 2002. Alteration of uraniferous and native copper concretions in the Permian mudrocks of south Devon, United Kingdom, Swedish Nuclear Fuel and Waste Management Company, Stockholm.

Morris, R.C. (2003) Iron ore genesis and post-ore metasomatism at Mount Tom Price. *Transactions of the Institutions of Mining and Metallurgy: Section B*, **112,** 56-67.

Morris, R.C. (2012) Microplaty hematite—its varied nature and genesis. *Australian Journal of Earth Sciences*, **59,** 411-434.

Mory, A.J. and Hocking, R.M. 2008. Geology of the Kalbarri and Mingenew Areas - A Field Guide, Geological Survey of Western Australia, Perth, Western Australia.

Mory, A.J., Iasky, R.P. and Ghori, K.A.R. 2003. A summary of the geological evolution and petroleum potential of the Southern Carnarvon Basin, Western Australia, Western Australia Geological Survey, Perth.

Mozley, P.S. (1996) The internal structure of carbonate concretions in mudrocks: a critical evaluation of the conventional concentric model of concretion growth. *Sedimentary Geology*, **103,** 85-91.

Mykura, H. and Hampton, B.P. (1984) On the mechanism of formation of reduction spots in the Carboniferous/Permian red beds of Warwickshire. *Geological Magazine*, 71-74.

Parnell, J. (2017) Tellurium and Selenium in Mesoproterozoic red beds. *Precambrian Research*, **305,** 145-150.

Parnell, J., Brolly, C., Spinks, S. and Bowden, S. (2015a) Metalliferous Biosignatures for Deep Subsurface Microbial Activity. *Origins of Life and Evolution of Biospheres*, **46,** 107-118.

Parnell, J., Spinks, S. and Bellis, D. (2016) Low-temperature concentration of tellurium and gold in continental red bed successions. *Terra Nova*, 221-227.

Parnell, J., Spinks, S. and Brolly, C. (2018) Tellurium and selenium in Mesoproterozoic red beds. *Precambrian Research*, **305,** 145-150.

Parnell, J., Still, J., Spinks, S. and Bellis, D. (2015b) Gold in Devono-Carboniferous red beds of northern Britain. *Journal of the Geological Society*, **173,** 245–248.

Parry, W.T., Chan, M.A. and Beitler, B. (2004) Chemical bleaching indicates episodes of fluid flow in deformation bands in sandstone. *AAPG Bulletin*, **88,** 175-191.

Pettijohn, F.J. (1963) Chemical Composition of Sandstones - Excluding Carbonate and Volcanic Sands. In: *Data of Geochemistry* (Ed M. Fleischer), **440**, pp. 1-21. US Government Printing Office, Washington, DC.

Plet, C., Grice, K., Pagès, A., Ruebsam, W., Coolen, M.J.L. and Schwark, L. (2016) Microbially-mediated fossil-bearing carbonate concretions and their significance for palaeoenvironmental reconstructions: A multi-proxy organic and inorganic geochemical appraisal. *Chemical Geology*, **426,** 95-108.

Salama, W. (2014) Paleoenvironmental significance of aluminum phosphate-sulfate minerals in the upper Cretaceous ooidal ironstones, E-NE Aswan area, southern Egypt. *International Journal of Earth Sciences*, **103,** 1621-1639.

Schulz, H., Wirth, R. and Schreiber, A. (2016) Nano-Crystal Formation of TiO2 Polymorphs Brookite and Anatase Due To Organic-Inorganic Rock-Fluid Interactions. *Journal of Sedimentary Research*, **86,** 59-72.

Schwertmann, U. and Latham, M. (1986) Properties of iron oxides in some New Caledonian oxisols. *Geoderma*, **39,** 105-123.

Spinks, S., Parnell, J. and Bowden, S.A. (2010) Reduction spots in the Mesoproterozoic age: implications for life in the early terrestrial record. *International Journal of Astrobiology*, **9,** 209-216.

Spinks, S., Parnell, J. and Still, J.W. (2014) Redox-controlled selenide mineralization in the Upper Old Red Sandstone. *Scottish Journal of Geology*, **50,** 173-182.

Spinks, S., Schmid, S., White, A.J., Parnell, J., Brolly, C., Pagès, A. and Revie, D. (in review) Head for the red beds! Earth's earliest colonisation of terrestrial environments by iron-reducing bacteria.

Srodon, J. (1980) Precise Identification of Illite/Smectite Interstratifications by X-ray Powder Diffraction. *Clays and Clay Minerals*, **28,** 401-411.

Sugitani, K., Horiuchi, Y., Adachi, M. and Sugisaku, R. (1996) Anomalously low Al_2O_3/TiO_2 values for Archean cherts from the Pilbara Block, Western Australia - possible evidence for extensive chemical weathering on the early earth. *Precambrian Research*, **80,** 49-76.

Thompson, D.R., Allwood, A., Assaid, C., Flannery, D., Hodyss, R., Knowles, E. and Wade, L. (2014) Adaptive Sampling for Rover X-ray Lithochemistry. In: *International Symposium on Artificial Intelligence, Robotics, and Automation in Space*, Montreal.

Trewin, N.H. (1993a) Controls on fluvial deposition in mixed fluvial and aeolian facies within the Tumblagooda Sandstone (Late Silurian) of Western Australia. *Sedimentary Geology*, **85,** 387-400.

Trewin, N.H. (1993b) Mixed aeolian sandsheet and fluvial deposits in the Tumblagooda Sandstone, Western Australia. In: *Characterisation of Fluvial and Aeolian Resevoirs*, pp. 219-230. Geological Society of London, London, UK.

Trewin, N.H. and Fallick, A.E. (2000) Quartz cement origins and budget in the Tumblagooda Sandstone, Western Australia. In: *Quartz Cementation in Sandstones* (Eds R.H. Worden and S. Morad). Wiley-Blackwell, Hoboken, USA.

Trewin, N.H. and McNamara, K.J. (1995) Arthropods invade the land: trace fossils and palaeoenvironments of the Tumblagooda Sandstone (?late Silurian) of Kalbarri, Western Australia. *Transactions of the Royal Society of Edinburgh: Earth Sciences*, **85,** 177-210.

Van Panhuys-Sigler, M., Trewin, N.H. and Still, J. (1996) Roscoelite associated with reduction spots in Devonian red beds, Gamrie Bay, Banffshire. *Scottish Journal of Geology*, **32,** 127-132.
Walker, T.R. (1967) Formation of Red Beds in Modern and Ancient Deserts. *Geological Society of America Bulletin*, **78,** 353-368.
Weaver, C.E. (1958) A discussion on the origin of clay minerals in sedimentary rocks. *Clays and clay minerals*, **5,** 159-173.
Weber, K.A., Achenbach, L.A. and Coates, J.D. (2006) Microorganisms pumping iron: anaerobic microbial iron oxidation and reduction. *Nature Reviews Microbiology*, 752-764.
Worden, R.H. and Morad, S. (2003) Clay minerals in sandstones: controls on formation, distribution, and evolution. In: *Clay Mineral Cements in Sandstones* (Eds R.H. Worden and S. Morad). Blackwell Publishing, Oxford, UK.

List of figures

Figure 1 – Montage of representative reduction spheroids observed within the Tumblagooda Sandstone. A and B are reduction spheroids observed within the sandstone of the Facies Association 3 with relatively small, zoned, and less mineralised cores. C and D are reduction spheroids with larger, darker, and more densely mineralised cores observed in siltstones within Facies Association 4.

Figure 2 – Map of the tectonic units along the Western Australian margin, modified from Mory and Hocking (2008).

Figure 3 – A. Map of the regional geology and extent of the Tumblagooda Sandstone around the Kalbarri townsite, modified from Martin et al. (2016). Note here, the letters next to formation names indicate formation ages and the black box surrounding the Kalbarri townsite represents the area in Figure 3b. Map (B) and satellite photograph (C) of the coastal exposures of the Tumblagooda Sandstone studied.

Figure 4 – Stratigraphic log of FA1-4 of the Tumblagooda Sandstone at Red Bluff. Beds known to host reduction spheroids are indicated. Modified from Trewin and McNamara

(1995). Note here that the thickness of the Gabba Gabba Member is intentionally exaggerated so as to ensure it is visible within the section due to its importance as a marker bed. Additionally, the abbreviations RVU and RBU are acronyms for *Rainbow Valley unit* and *Red Bluff unit* and are discussed on page 10.

Figure 5 – X-ray computed tomography scan of two whole reduction spheroids, displaying their three-dimensional nature and a spheroidal core composed of higher density minerals. The scanned material is coloured red, green, blue, and grey in order of decreasing density. Sampled from the Red Bluff Unit (FA3).

Figure 6 – SEM photomicrographs of mineral phases within the Tumblagooda Sandstone reduction spheroids. A. Backscattered electron (BSE) image of dense interstitial microplaty haematite (MplH) that occurs throughout the reduction spheroid cores between grains of quartz (Qz) and microcline (Mc). B. Secondary electron (SE) image of the microplaty haematite that occurs within the reduction spheroid cores. C. BSE image of microplaty haematite occurring in proximity to intergrown fine haematite (haem) and the illite (Ilt) matrix that is common outside of the reduction spheroid cores. D. BSE image of mixed fine haematite and illite that is common throughout red portions of reduction spheroid cores. E. BSE image of a cluster of acicular authigenic anatase (Ant). F. BSE image of a grain with titaniferous laths arranged in a trellis-like orientation. G. BSE image of relatively coarse blocky authigenic anatase occurring within a reduction spheroid core, proximal to microplaty haematite. H. BSE image of two distinct morphologies of authigenic anatase occurring in proximity to one another. One type is very fine and granular whilst the other is relatively coarse and typically blocky.

Figure 7 – A. BSE image of a grain of authigenic anatase with inclusions of uraninite (Urn). B. Typical BSE image of a portion of the pale reduced zone within a given reduction spheroid; interstitial areas are dominated by an illite matrix with dispersed svanbergite. C. BSE image of a cluster of fine authigenic svanbergite grains occurring in a void within a quartz grain. D. BSE image of a cubic grain of svanbergite (Sva) zoned with an outer gorceixite (Gor) rim, the dashed line indicates the boundary between these two compositions. E. BSE image of fine authigenic monazite (Mnz) that occurs within some reduction spheroids around the edges of quartz grains. In this case, they occur in line with voids in an overgrown quartz grain that may be a product monazite that grew around the edge and has since been removed. F. BSE image of a typical unaltered detrital ilmenite grain that occurs within the host Tumblagooda Sandstone but not in the reduction spheroids, note the primary magmatic exsolution textures between Fe and Ti-rich portions.

Figure 8 – A. Mosaic of RBU-RS-50. B. XRF map of a RBU-RS-50; a reduction spheroid core retrieved from the RBU of the Tumblagooda Sandstone showing distribution of Si, K, Fe, and Ti. Here it is clear that haematite (Fe) occurs as an interstitial component between detrital quartz (Si) and K-feldspar (K), with Ti-bearing phases occurring along the prevailing sedimentary fabric. C. Mosaic of RVU-RS-55. D. XRF map of a RVU-RS-55; a reduction spheroid core retrieved from the RBU of the Tumblagooda Sandstone displaying Si, K, Fe, and Ti. E. XRF map of RVU-RS-55; displaying Fe diffusion along sedimentary fabric away from Fe-rich core.

Figure 9 – Paragenetic sequence of the formation of the Tumblagooda Sandstone reduction spheroids from petrographic analysis. Here the genesis of these reduction spheroids is broken into three stages. Stage one: the initial formation of the reduction

spheroids and active bacterial metal reduction. Stage two: the cessation of active bacterial metal reduction and the subsequent oxidation and heating of the reduction spheroids during burial. Stage three: the exhumation of the reduction spheroids within the wider Tumblagooda Sandstone and their exposure to concomitantly lower temperatures. Note here that the change in colour from blue in stage one to red in stage two is indicative of the progressive heating of the reduction spheroids during burial.

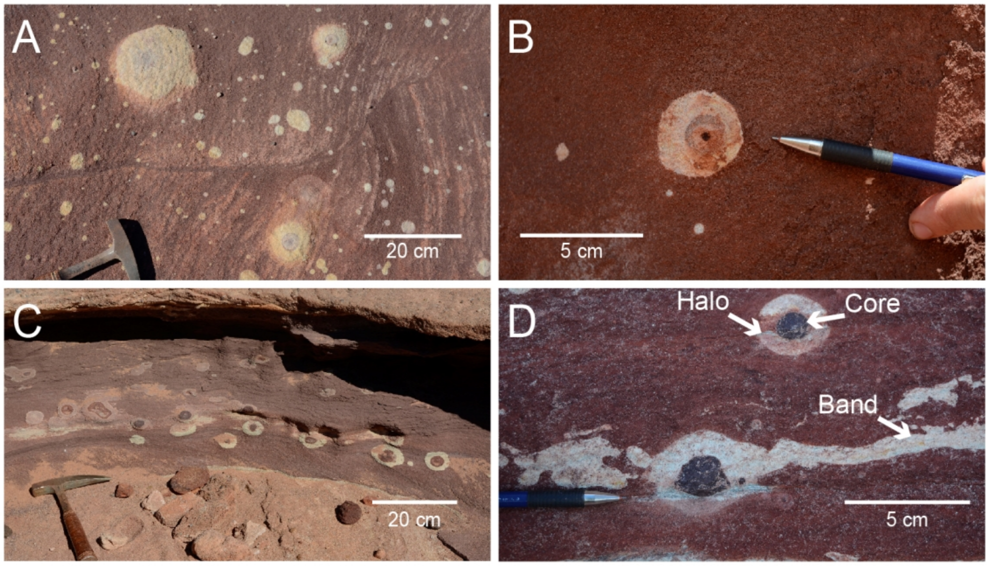

C:\Users\17089313\OneDrive - Curtin University of Technology Australia\PhD\Papers\Tumblagooda RS Summary\Part One\Review\Figures\PNG

140x79mm (300 x 300 DPI)

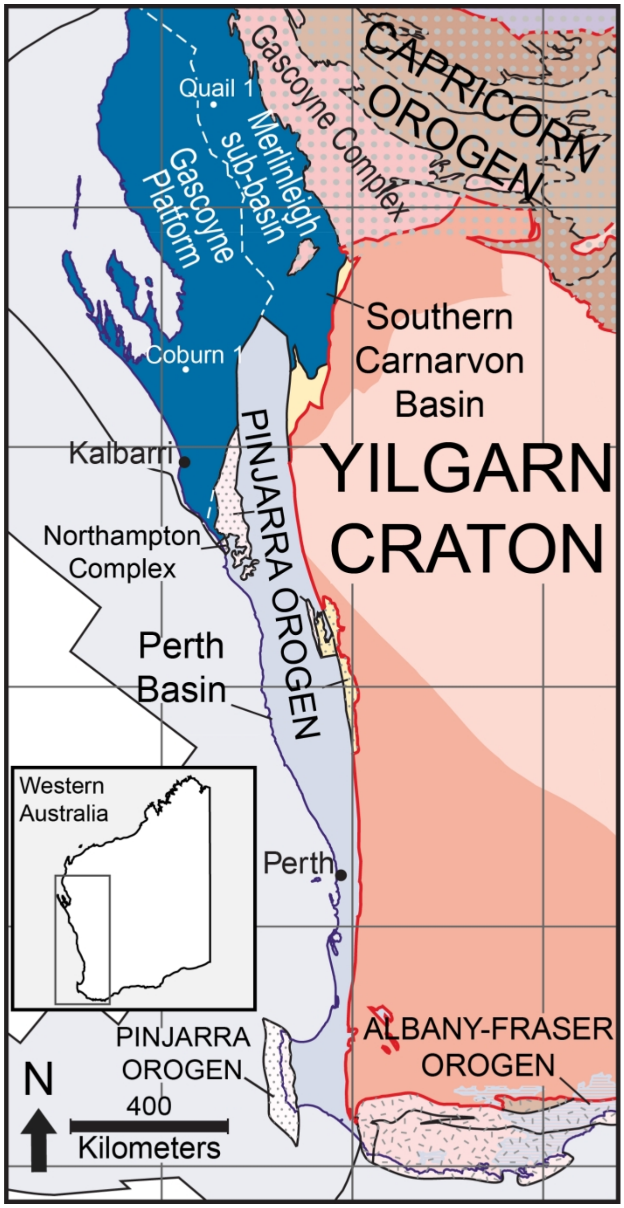

Figure 2 – Map of the tectonic units along the Western Australian margin, modified from Mory and Hocking (2008).

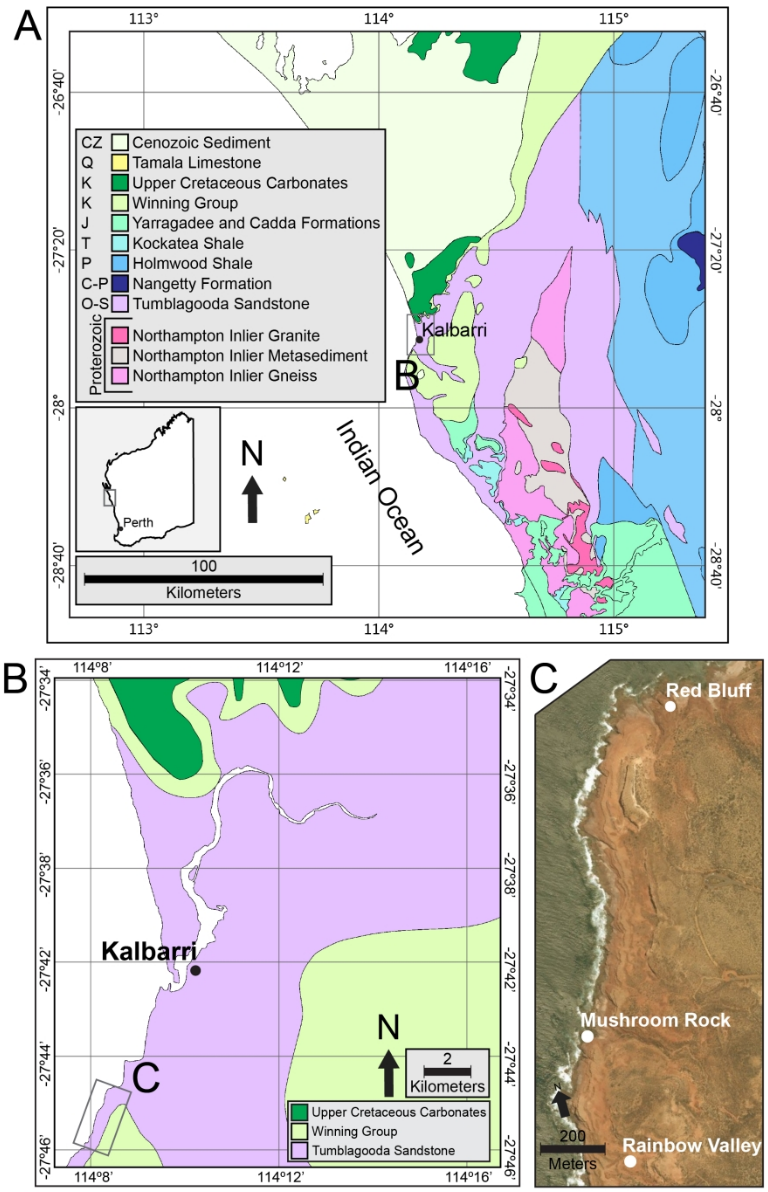

Figure 3 - A. Map of the regional geology and extent of the Tumblagooda Sandstone around the Kalbarri townsite, modified from Martin et al. (2016). Note here, the letters next to formation names indicate formation ages and the black box surrounding the Kalbarri townsite represents the area in Figure 2b. Map (B) and satellite photograph (C) of the coastal exposures of the Tumblagooda Sandstone studied.

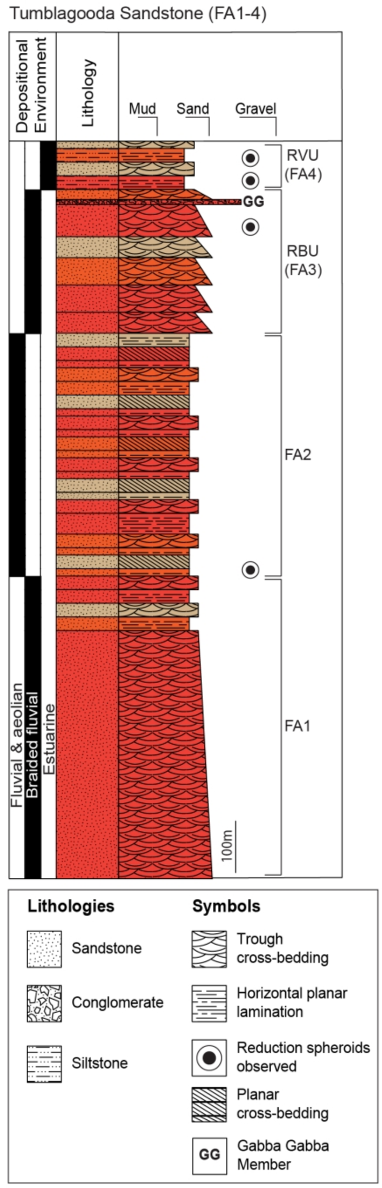

Figure 4 – Stratigraphic log of FA1-4 of the Tumblagooda Sandstone at Red Bluff. Beds known to host reduction spheroids are indicated. Modified from Trewin and McNamara (1995). Note here that the thickness of the Gabba Gabba Member is intentionally exaggerated so as to ensure it is visible within the section due to its importance as a marker bed. Additionally, the abbreviations RVU and RBU are acronyms for Rainbow Valley unit and Red Bluff unit and are discussed on page 10.

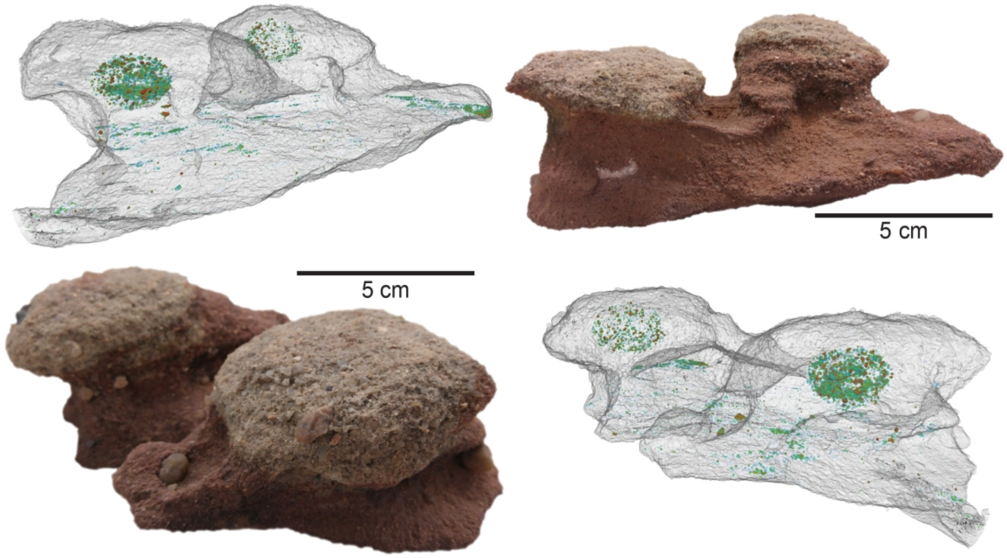

Figure 5 – X-ray computed tomography scan of two whole reduction spheroids, displaying their three-dimensional nature and a spheroidal core composed of higher density minerals. The scanned material is coloured red, green, blue, and grey in order of decreasing density. Sampled from the Red Bluff Unit (FA3).

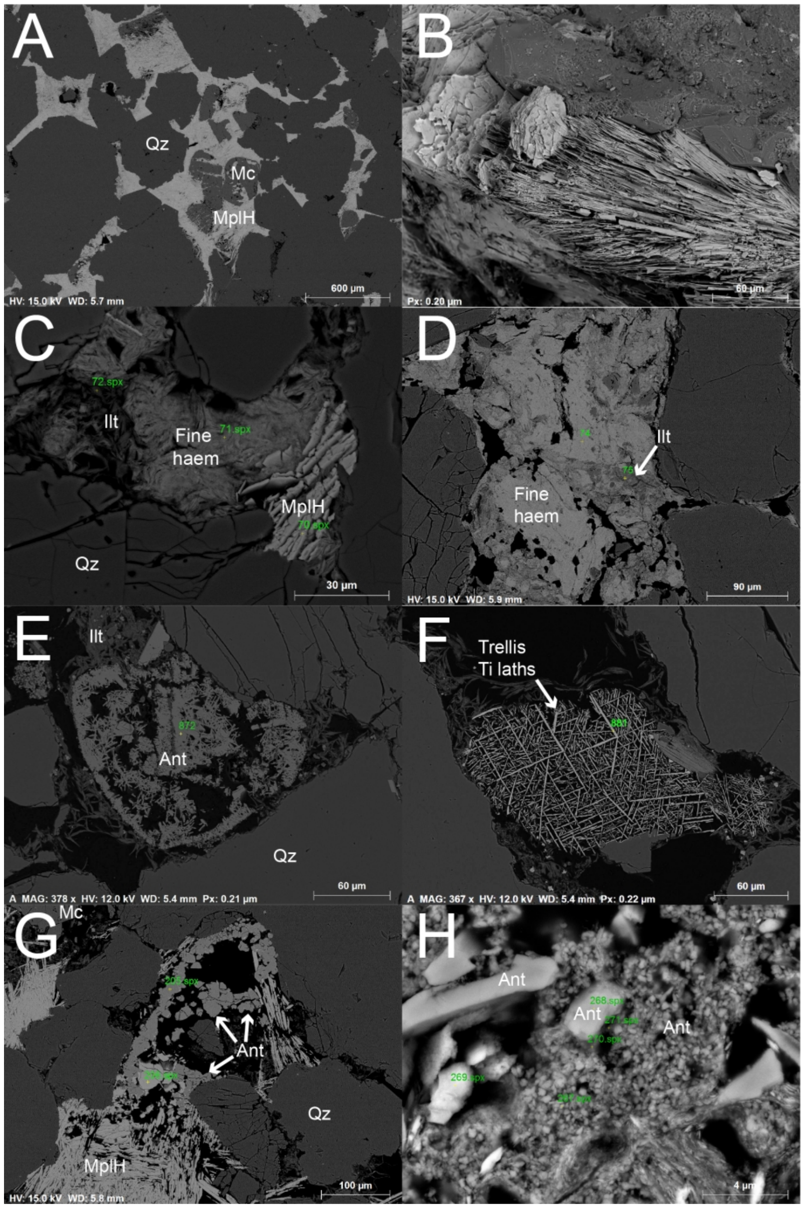

Figure 6 – SEM photomicrographs of mineral phases within the Tumblagooda Sandstone reduction spheroids. A. Backscattered electron (BSE) image of dense interstitial microplaty haematite (MplH) that occurs throughout the reduction spheroid cores between grains of quartz (Qz) and microcline (Mc). B. Secondary electron (SE) image of the microplaty haematite that occurs within the reduction spheroid cores. C. BSE image of microplaty haematite occurring in proximity to intergrown fine haematite (haem) and the illite (Ilt) matrix that is common outside of the reduction spheroid cores. D. BSE image of mixed fine haematite and illite that is common throughout red portions of reduction spheroid cores. E. BSE image of a cluster of acicular authigenic anatase (Ant). F. BSE image of a grain with titaniferous laths arranged in a trellis-like orientation. G. BSE image of relatively coarse blocky authigenic anatase occurring within a reduction spheroid core, proximal to microplaty haematite. H. BSE image of two distinct morphologies of authigenic anatase occurring in proximity to one another. One type is very fine and granular whilst the other is relatively coarse and typically blocky.

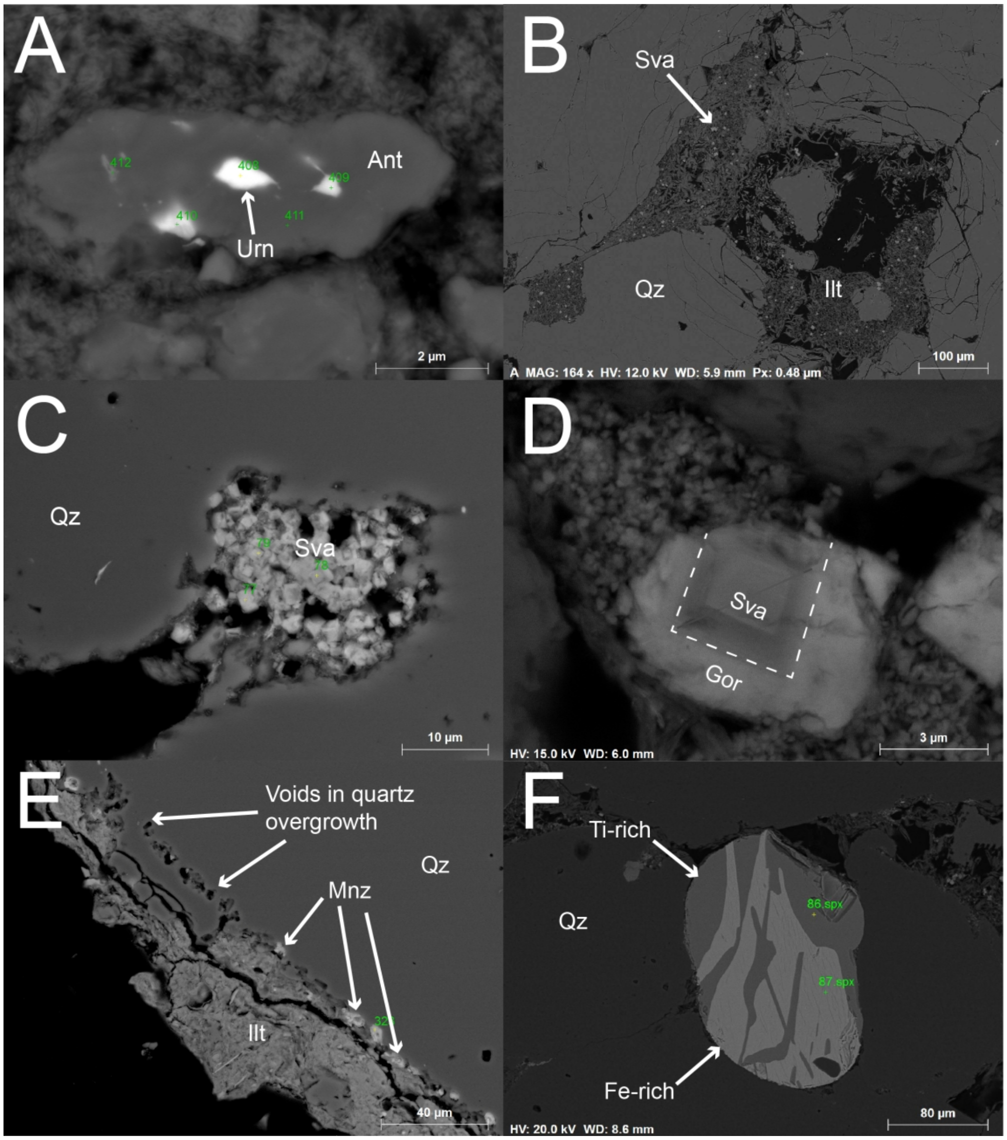

Figure 7 – A. BSE image of a grain of authigenic anatase with inclusions of uraninite (Urn). B. Typical BSE image of a portion of the pale reduced zone within a given reduction spheroid; interstitial areas are dominated by an illite matrix with dispersed svanbergite. C. BSE image of a cluster of fine authigenic svanbergite grains occurring in a void within a quartz grain. D. BSE image of a cubic grain of svanbergite (Sva) zoned with an outer gorceixite (Gor) rim, the dashed line indicates the boundary between these two compositions. E. BSE image of fine authigenic monazite (Mnz) that occurs within some reduction spheroids around the edges of quartz grains. In this case, they occur in line with voids in an overgrown quartz grain that may be a product monazite that grew around the edge and has since been removed. F. BSE image of a typical unaltered detrital ilmenite grain that occurs within the host Tumblagooda Sandstone but not in the reduction spheroids, note the primary magmatic exsolution textures between Fe and Ti-rich portions.

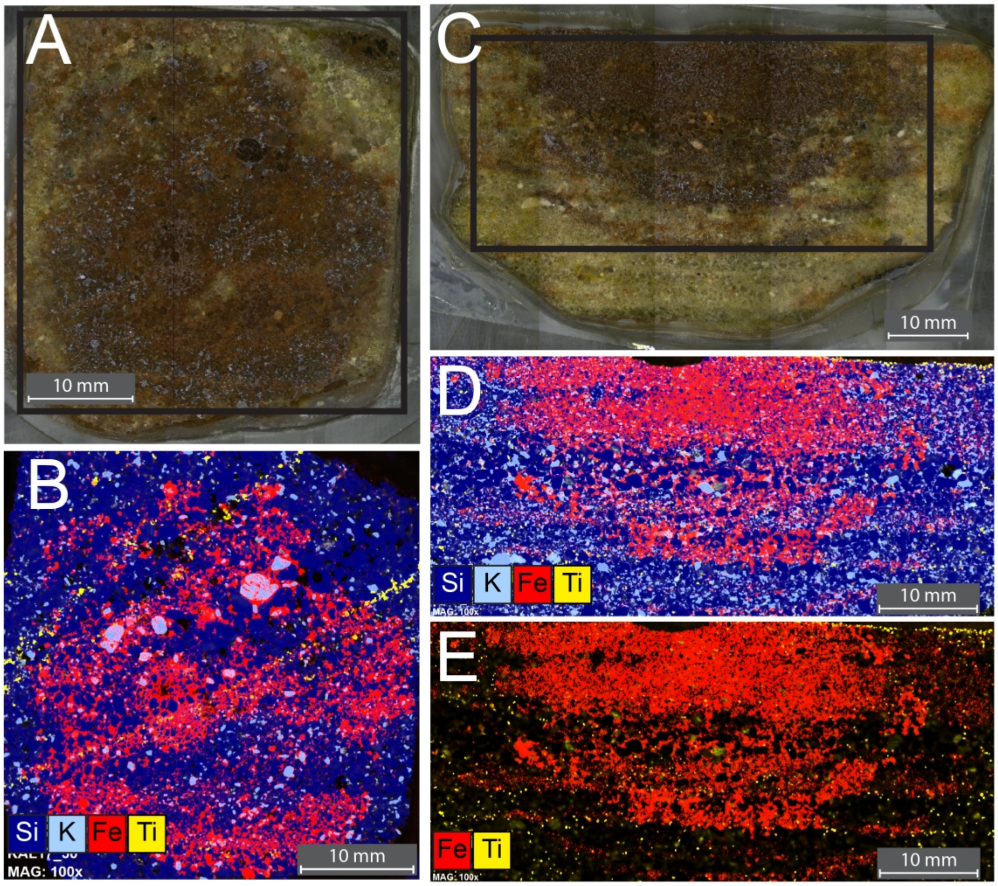

Figure 8 – A. Mosaic of RBU-RS-50. B. XRF map of a RBU-RS-50; a reduction spheroid core retrieved from the RBU of the Tumblagooda Sandstone showing distribution of Si, K, Fe, and Ti. Here it is clear that haematite (Fe) occurs as an interstitial component between detrital quartz (Si) and K-feldspar (K), with Ti-bearing phases occurring along the prevailing sedimentary fabric. C. Mosaic of RVU-RS-55. D. XRF map of a RVU-RS-55; a reduction spheroid core retrieved from the RBU of the Tumblagooda Sandstone displaying Si, K, Fe, and Ti. E. XRF map of RVU-RS-55; displaying Fe diffusion along sedimentary fabric away from Fe-rich core.

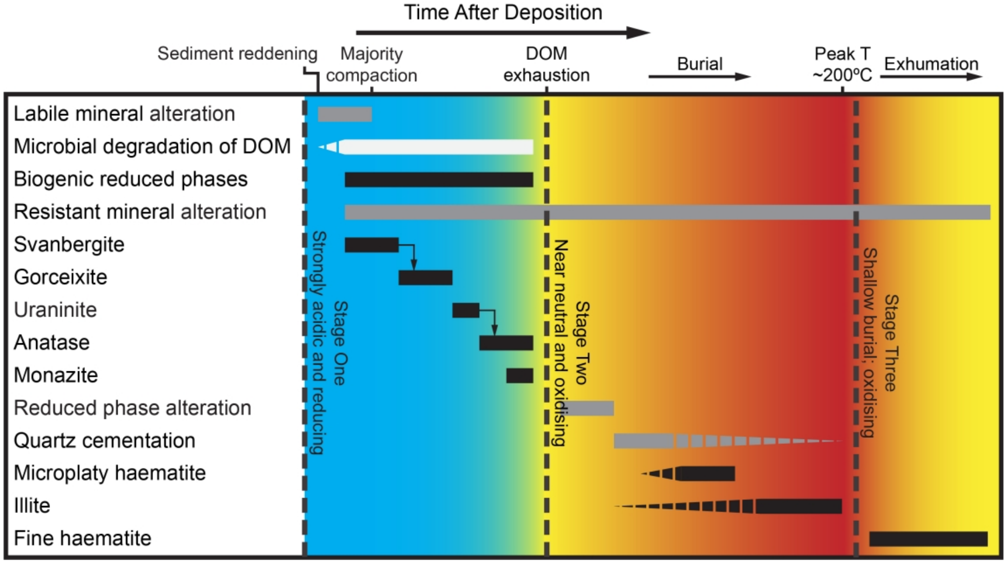

Figure 9 – Paragenetic sequence of the formation of the Tumblagooda Sandstone reduction spheroids from petrographic analysis. Here the genesis of these reduction spheroids is broken into three stages. Stage one: the initial formation of the reduction spheroids and active bacterial metal reduction. Stage two: the cessation of active bacterial metal reduction and the subsequent oxidation and heating of the reduction spheroids during burial. Stage three: the exhumation of the reduction spheroids within the wider Tumblagooda Sandstone and their exposure to concomitantly lower temperatures. Note here that the change in colour from blue in stage one to red in stage two is indicative of the progressive heating of the reduction spheroids during burial.

Table 1 - Summary of minerals with abundance and nature of occurrence in host Tumblagooda Sandstone and reduction spheroids.

Mineral phase	Abundance and nature of occurrence
Quartz	Common. Primary. Dominant detrital mineral in host rock and throughout reduction spheroids.
K-feldspar	Common. Primary. Abundant detrital mineral in host rock and throughout reduction spheroids.
Heavy minerals	Common. Primary. Detrital zircon, monazite, ilmenite, and rutile common in red host sandstone. Detrital ilmenite, rutile, and monazite are rare in white sandstone and reduction spheroids.
Svanbergite	Common. Authigenic. Occurs throughout reduction spheroids in aggregates of cubic crystals filling interstitial space.
Gorceixite	Common. Authigenic. Occurs exclusively rimming svanbergite crystals.
Uraninite	Trace. Authigenic. Occurs exclusively as inclusions within anatase throughout spheroids.
Anatase	Trace. Authigenic. Occurs as clusters of acicular anatase needles in interstitial space in reduction spheroid cores with very fine (<1 μm) surrounding aggregates.
Monazite	Trace. Authigenic. Occurs as clusters of crystals (<10 μm) commonly adhered to detrital quartz grains in reduction spheroid cores.
Microplaty haematite (MplH)	Common. Authigenic. Dominates interstitial space through majority of reduction spheroid cores.
Illite	Common. Authigenic. Dominates interstitial space in reduction spheroid halos and host rock, also occurs through less dense reddish cores.
Fine haematite	Common, occurs in association with MplH in reddish cores and commonly intergrown with illite.

Summary of minerals with abundance and nature of occurrence in host Tumblagooda Sandstone and reduction spheroids